

Shell-structure-based functionals for the kinetic energy

K. Finzel¹

Received: 25 May 2015 / Accepted: 29 July 2015 / Published online: 15 August 2015
© Springer-Verlag Berlin Heidelberg 2015

Abstract A new group of shell-structure-based functionals, which rely on proper representation of the atomic shell structure in real space, is introduced. Starting from the model of a perfect piecewise exponential decaying electron density, an analytical expression for the kinetic energy density including two parameters is given. It is shown that parameter values which lead to a proper shell structure in real space give rise to suitable kinetic energy functionals.

Keywords Orbital-free DFT · Atomic shell structure · Pauli potential · Kinetic energy density · Atoms

1 Introduction

Orbital-free density-functional theory has gained much interest in recent years [1–5], as it promises a reliable physical description of the system at very low computational cost. The main challenge for a widespread use of orbital-free density-functional theory is to find sufficiently accurate approximations for the kinetic energy. Besides well-known approximations as given by Thomas [6] and Fermi [7], the von Weizsäcker functional [8] or the gradient expansion [9, 10], much effort has been undertaken in the direction of generalized gradient approximations motivated by conjoint arguments [11], information-theory-motivated functionals [12–14] or functionals based on response theory [4, 15]. The presented study provides another route for the design of kinetic energy functionals, which are based

on the correct treatment of the atomic shell structure [16–22]. Based on the knowledge of the atomic shell structure in terms of the electronic density and its gradient [21, 23], improved kinetic energy functionals can be constructed incorporating the atomic shell effect, which has been shown to play an important role [24] for densities obtained from the Hohenberg–Kohn variational principle [25].

The motivation to design kinetic energy functionals yielding self-consistent densities from Hohenberg–Kohn variational principle [25] dates back to 1965 when Yonei and Tomishima [26] showed that Thomas–Fermi–Weizsäcker functionals (TFW) of the form:

$$T[\rho] = T_{\text{TF}}[\rho] + \lambda T_{\text{W}}[\rho] \quad (1)$$

are not able to yield self-consistent electron densities exhibiting atomic shell structure irrespective of the chosen weighting factor λ . In the above expression, the Thomas–Fermi term [6, 7] is:

$$T_{\text{TF}}[\rho] = \int t_{\text{TF}}(\mathbf{r}) \, d\mathbf{r} = \int c_F \rho(\mathbf{r})^{5/3} \, d\mathbf{r}, \quad (2)$$

with the Fermi constant $c_F = 3/10(3\pi^2)^{2/3}$ and $\rho(\mathbf{r})$ being the electron density of the system. The von Weizsäcker term [8] is given by:

$$T_{\text{W}}[\rho] = \int t_{\text{W}}(\mathbf{r}) \, d\mathbf{r} = \frac{1}{8} \int \frac{(\nabla \rho(\mathbf{r}))^2}{\rho(\mathbf{r})} \, d\mathbf{r}. \quad (3)$$

Later on, the local properties of the gradient expansion of the kinetic energy density including the effect of additive density Laplacian contributions were intensively studied [27–30], but it turned out that none of the proposed functionals yield self-consistent densities showing the proper atomic shell structure, although some of the proposed approximations seemed to be promisingly close to

✉ K. Finzel
kati.finzel@cpfs.mpg.de; kati.finzel@liu.se

¹ IFM, Linköpings Universitetet, Fysikhuset, 58183 Linköping, Sweden

the positive kinetic energy density obtained from a Slater determinant [29, 30].

A promising report about how to obtain self-consistent atomic densities exhibiting proper atomic shell structure from the Hohenberg–Kohn variational principle using a simple functional for the kinetic energy was given by Deb and Ghosh [24]. In that work the positive kinetic energy density:

$$\tau(\mathbf{r}) = t_W + f(\mathbf{r})t_{TF}, \quad (4)$$

was constructed from the full von Weizsäcker term and a modified Thomas–Fermi term, with locally varying correction factor $f(\mathbf{r})$. That correction factor was later and in a different context known as the kernel of the electron localization function (ELF) [31], originally developed by Becke and Edgecombe [32]. However, Deb and Ghosh did not provide an analytical formula for their correcting function $f(\mathbf{r})$, but mimicked it by a fit of superposed Gaussian functions, which had to be stored for each atom separately. Thus, the question remained how to express $f(\mathbf{r})$ by a purely density-based ansatz.

The close connection between ELF and the local behavior of a given approximation for $T[\rho]$ can also be stated by the following argument. Kinetic energy functionals of GGA type can be written as [1]

$$T[\rho] = \int t_{TF} F_t(s) d\mathbf{r}, \quad (5)$$

whereby the enhancement factor F_t is usually considered to be a function of the reduced density gradient $s = 1/(2(3\pi^2))^{1/3} |\nabla\rho|/\rho^{4/3}$. Writing down an equivalent expression [1] for the Pauli term $T_P = T - T_W$:

$$T_P[\rho] = \int t_{TF} F_P(s) d\mathbf{r} \quad (6)$$

immediately reveals that the enhancement factor F_P is nothing else but the kernel of the ELF, since:

$$T_P[\rho] = \int t_P d\mathbf{r} = \int t_{TF} \frac{\tau - t_W}{t_{TF}} d\mathbf{r}. \quad (7)$$

Therefore, purely density-based functions being reasonably close to ELF give rise to new kinetic energy functionals. Those functionals will be termed shell-structure-based (SSB) functionals. One possible group of such functionals based on the approximation of ELF with the help of the charge-restricted density-inhomogeneity measure (dim-q) will be presented in this work.

Note, that the following work presents a strategy how to obtain orbital-free kinetic energy functionals starting from orbital-free atomic shell descriptors. The reverse strategy obtaining density-based atomic shell descriptors as well as bonding indices using orbital-free approaches for the

kinetic energy density has been intensively studied in the literature [33–37].

2 Conceptual remarks

In the design of kinetic energy functionals, the aim is to approximate either $T[\rho]$ or $T_s[\rho]$, whereby $T[\rho]$ is the exact kinetic energy of the electronic system and $T_s[\rho]$ is the kinetic energy for the corresponding noninteracting system with the same density ρ [38]. The two quantities are related by the rigorous inequality ($T > T_s$) [39]. On the other hand, there is the kinetic energy as given by Hartree–Fock (HF) theory $T^{HF}[\rho^{HF}]$, whereby the difference to the exact kinetic energy is minus the conventional quantum mechanical correlation energy E_c [40]. The noninteracting kinetic energy from Kohn–Sham (KS) theory evaluated for the HF density is always lower than the corresponding HF kinetic energy ($T^{HF}[\rho^{HF}] > T_s[\rho^{HF}]$), due to the difference between the HF and KS orbitals, but their numerical difference is small. An elusive study as well as numerical results can be found in Refs. [39, 41].

However, the major challenge in the design of a kinetic energy functional is an adequate estimate of the extra kinetic energy required by the Pauli exclusion principle ($T_s[\rho] = T_W[\rho] + T_P[\rho]$), which can be of the same order of magnitude as $T_W[\rho]$ itself. Since this study is exclusively devoted to approximations of $T_P[\rho]$, differences in the kinetic energy due to correlation as well as due to the influence of the method (KS or HF) on the orbitals are safely ignored. As will be shown, errors due to the explicit functional expressions are much larger than those of the above-mentioned factors. For atomic calculations, functional expressions will be evaluated for the HF density $T_{test}[\rho^{HF}]$ and compared to $T^{HF}[\rho^{HF}]$, irrespective of whether they have been aimed to approximate $T[\rho]$ or $T_s[\rho]$.

A similar argument applies to the investigations of the ELF kernel and its density-based approximations evaluated from t_{test} . Differences in ELF when evaluated from KS orbitals and HF orbitals, respectively, are negligible [42] compared with the influence of the density approximations for t_{test} on the resulting approximative ELF kernels. In correspondence with the treatment of $T_{test}[\rho^{HF}]$, the ELF kernel and approximative ELF kernels for atomic calculations are evaluated from HF results.

Finally, it should be mentioned that there is no guarantee that a given kinetic energy functional providing reasonable energies using proper test densities (from HF or KS calculations) will also yield those densities when applied with the Hohenberg–Kohn variational principle; see, for example, the work of Yonei and Tomishima [26].

3 Computational details

The calculations of properties were performed with a modified version of DGrid [43]. If not stated otherwise, the majority spin component has been evaluated. Atomic calculations are based on the HF wavefunctions of Clementi and Roetti [44]. For the solid-state calculations of Si in the diamond structure ($Fd\bar{3}m$ with $a = 10.1586$ bohr), the ELK code [45] was used. Atomic units are used throughout this work.

4 Results

4.1 Information-theory-based and GGA-type functionals

Having made the connection between the kernel of the ELF and the Pauli enhancement factor F_P for a given kinetic energy functional, it suffices to compare those enhancement factors directly with the ELF kernel in order to judge the atomic shell performance of that functional for a given atom. Every kinetic energy functional $T_{\text{test}}[\rho]$ of the form $T_{\text{test}}[\rho] = \int t_{\text{test}}(\mathbf{r}) d\mathbf{r}$ leads to a so-called approximative ELF kernel elf_{test} , when τ of the original ELF kernel [31] is replaced by the approximative kinetic energy density $t_{\text{test}}(\mathbf{r})$. In order to exhibit the proper shell structure for a given atom, the Pauli enhancement factor of a kinetic energy functional must have its extrema nearby the corresponding extremal positions of the ELF kernel. Those enhancement factors whose whole topology is also reasonably close to the one of the ELF kernel, meaning that the values of the original elf_τ evaluated from orbitals are also sufficiently well reproduced by the density-based approximation elf_{test} , will yield good approximations for the local kinetic energy density and therefore for total kinetic energy as well.

In this study, the local behavior of Pauli enhancement factors for two types of frequently used functional forms, namely the information-theory-motivated functionals and the kinetic energy functionals of GGA type, respectively, will be examined. Information-theoretic kinetic energy functionals, such as T_{GDS08} [12], T_{GHDS10} [13] and T_{TKVln} [14], can be written in the form:

$$T[\rho] = aT_W[\rho] + bT_{\text{TF}}[\rho] + \int \rho[c + d \ln \rho + e \ln^2 \rho] d\mathbf{r}, \quad (8)$$

whereby the spin-polarized formulas have been obtained by setting:

$$T[\rho^\sigma] = \frac{1}{2} T[2\rho^\sigma]. \quad (9)$$

Spin-polarized approximative ELF kernels are derived in the same way like the spin-polarized formula for the ELF kernel as introduced by Kohout and Savin [20]:

$$\text{elf}_{\text{test}} = \frac{t_{\text{test}}^\alpha + t_{\text{test}}^\beta - t_W^\alpha - t_W^\beta}{t_{\text{TF}}^\alpha + t_{\text{TF}}^\beta}. \quad (10)$$

By using the above scheme, the function $\text{elf}_{\text{GDS08}}$ is the approximative ELF kernel generated by the local kinetic energy density of the T_{GDS08} kinetic energy functional [12], with $a = 1, b = 0, c = 0.860, d = 0.224, e = 0$. Likewise, we construct $\text{elf}_{\text{GHDS10}}$ from T_{GDS10} [13], whereby the original parameters from Ghiringhelli, Hamilton and Delle Site $a = 1, b = 1, c = 1.02, d = 0.163, e = 0$ are taken from [14] and $\text{elf}_{\text{GHDS10-repar}}$ by choosing the reparametrized set $a = 1, b = 1, c = 0.061434, d = 0.0061317, e = 0$ of Trickey, Karasiev and Vela [14]. The approximative ELF kernel $\text{elf}_{\text{TKVln}}$ with $a = 1, b = 1, c = 0.04, d = 0.0065545, e = 0.00023131$ has been obtained from the kinetic energy functional T_{TKVln} [14]. Similarly, elf_{TF} is constructed by setting $b = 1$ and the remaining coefficients to zero. Of course, the function elf_w , whereby the only nonzero coefficient is $a = 1$, is zero everywhere.

Besides that, the following GGA-type functionals were studied: the “conjoint” Perdew–Wang 91 functional T_{PW91} constructed by Lacks and Gordon [46]:

$$F_t^{\text{PW91}} = \frac{1 + 0.19645s \operatorname{arcsinh}[7.7956s] + [0.2743 - 0.1508e^{-100s^2}]s^2}{1 + 0.19645s \operatorname{arcsinh}[7.7956s] + 0.004s^4}, \quad (11)$$

the semiempirical functional proposed by DePristo and Kress T_{DPK} [47]:

$$F_t^{\text{DPK}} = \frac{1 + 0.95y + 14.2811y^2 - 19.57962y^3 + 26.6477y^4}{1 - 0.05y + 9.99802y^2 + 2.96085y^3}, \quad (12)$$

whereby:

$$y = \frac{t_W}{9t_{\text{TF}}}, \quad (13)$$

the functional introduced by Thakkar T_{Thakkar} [48]:

$$F_t^{\text{Thakkar}} = 1 + \frac{0.0055[bs]^2}{1 + 0.0253bs \operatorname{arcsinh}[bs]} - \frac{0.072[bs]^2}{1 + 2^{5/3}bs}, \quad (14)$$

with:

$$b = 2(6\pi^2)^{1/3} \quad (15)$$

and the reparametrized PBE functional $T_{\text{PBE-TW}}$ [11]:

$$F_t^{\text{PBE-TW}} = 1 + \frac{0.2319s^2}{1 + 0.2748s^2}. \quad (16)$$

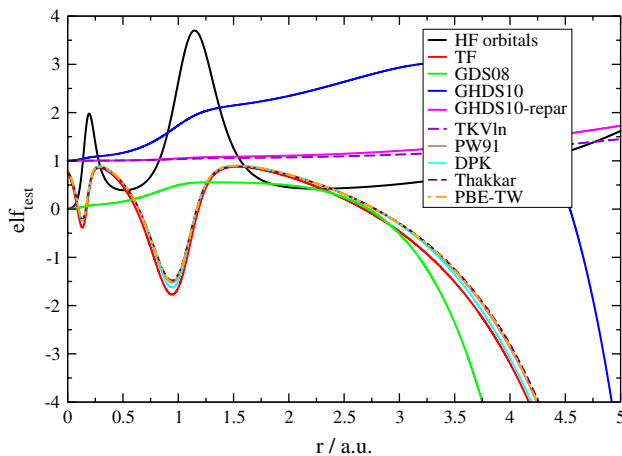


Fig. 1 Approximative ELF kernels for the majority spin channel for the Si atom obtained from the kinetic energy densities of various information-theory-motivated functionals and GGA-type functionals

Likewise, spin-polarized formulas for the kinetic energy densities have been obtained from Eq. (9) and spin-polarized approximative ELF kernels by using Eq. (10).

None of the approximative ELF kernels obtained from information-theoretic functionals or GGA-type functionals is able to reproduce the proper atomic shell structure, as shown in Fig. 1, where the approximative ELF kernels are given exemplarily for the Si atom. The approximative ELF kernels originating from the density-based ansatzes do not resemble the original ELF kernel obtained from orbitals. Figure 1 also reveals the close similarity of all GGA-type functionals, independent of the chosen functional form. All approximative ELF kernels of GGA-type functionals are in close vicinity to the ELF kernel from the pure Thomas–Fermi term, which means that all GGA-type functionals will have local kinetic energy densities closely resembling the pure t_{TF} , cf. Fig. 2. Therefore, all examined GGA-type functionals will yield similar results like the pure TF term, both with respect to the local behavior as well as energetics. This can be deduced also from Fig. 3, where the difference between the kinetic energy evaluated from orbitals and a given density-based approximation is plotted as a function of distance from the nucleus ($\Delta T(r) = \int_0^r 4\pi r^2 [t_{\text{test}}(r) - \tau(r)] dr$). The value at the right-hand side of the plot is practically identical to the difference in the kinetic energy between the two ansatzes, since as all $t_{\text{test}}(r)$ drop off very quickly with increasing r , the contribution to the total kinetic energy becomes marginal, and therefore, $\Delta T(r)$ quickly converges, even so, that the local kinetic energy densities might differ largely from each other at large distances; see, e.g., the $t_{\text{GDS08}}(r)$ in Fig. 2 and the corresponding $\Delta T(r)$ in Fig. 3.

The diagram $\Delta T(r)$ is especially useful when judging simultaneously the energetic performance of a given

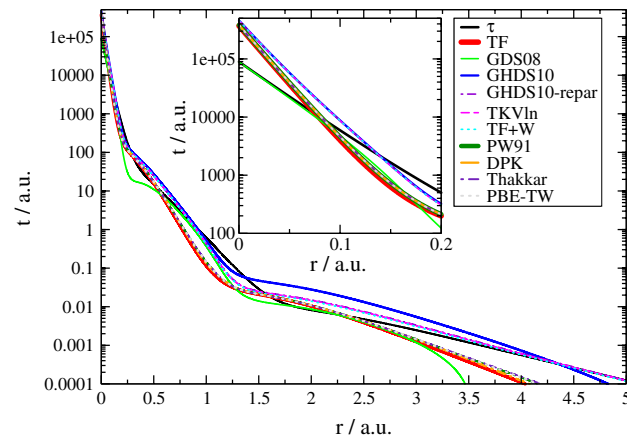


Fig. 2 Approximative kinetic energy densities for the majority spin channel for the Si atom using various information-theory-motivated functionals and GGA-type functionals

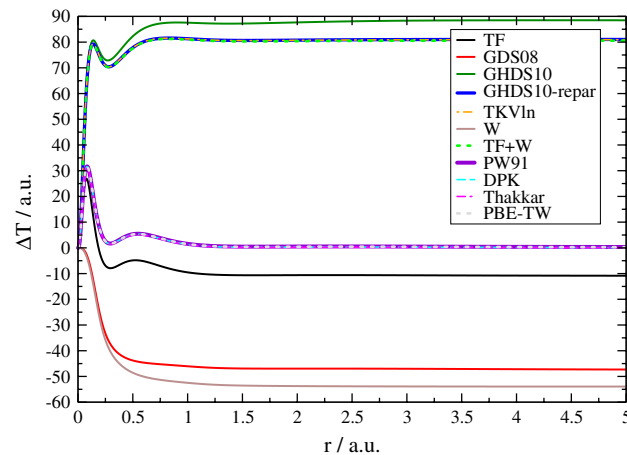


Fig. 3 Local contributions to the difference between the kinetic energy evaluated from orbitals and the approximative kinetic energy ($\Delta T(r) = \int_0^r 4\pi r^2 [t_{\text{test}}(r) - \tau(r)] dr$) for the Si atom using various information-theory-motivated functionals and GGA-type functionals

functional as well as its local performance of t_{test} . In principle, there is no need for a given functional form that t_{test} matches τ due to the ambiguity of the kinetic energy density itself [49–51], inferring that any kinetic energy density yielding the proper integral for the kinetic energy is an acceptable kinetic energy density, although its local form does not bear any resemblance with τ . However, if one wishes to approximate the kinetic energy density using piecewise ansatzes for different local regions, e.g., muffin-tin spheres and interstitial regions or any other local separation scheme, then a local correspondence between t_{test} and τ is important. Thus, the desired form for t_{test} should exhibit the smallest $\Delta T(r)$ oscillations as possible. As shown in Fig. 3, GGA-type functionals all perform well with respect

to the total energy, comparing also data in Table 1, since all curves are fairly close to zero at the right-hand side of the figure, but this goal has been obtained by deteriorating the local description in the vicinity of the Si nucleus, since the local dip of $\Delta T(r)$ is more pronounced than the corresponding dip for TF. This can be deduced from Fig. 2 as well, where all t_{test} for GGA-type functionals lie above the TF kinetic energy density, meaning that the better overall correspondence with T has been obtained by a supplementary overestimation of the kinetic energy density nearby the nucleus. The same is true for the tested information-theory-motivated functionals: They also overestimate the local kinetic energy nearby the nucleus, although their integrated values are worse than those of GGA type, except t_{GDS08} . The $T_{\text{GDS08}}[\rho]$ functional is the only one out of the examined set that shows the proper behavior close to the Si nucleus. This conclusion can also be drawn from the corresponding ELF kernels; see Fig. 1, where $\text{elf}_{\text{GDS08}}$ is the only function being close to the ELF kernel elf_t in the vicinity of the Si nucleus. However, the global behavior of $\text{elf}_{\text{GDS08}}(\mathbf{r})$ is not satisfactory, significantly underestimating the influence of the Pauli principle (all values are close to zero), and therefore, the corresponding $\Delta T(r)$ is very similar to the one obtained from the pure von Weizsäcker functional. By the way, $\text{elf}_{\text{GHDS10-repar}}$ and $\text{elf}_{\text{TKVln}}$ do not differ much from one over the whole range of r values and as a consequence of this the functions t_{test} do not differ much from the simple superposition of the TF and von Weizsäcker term, cf. Figs. 2 and 3, where the three curves for $T_{\text{GHDS10-repar}}$, T_{TKVln} and $T_{\text{TF+W}}$ cannot be distinguished.

4.2 Shell-structure-based functionals

Since the search is explicitly carried out for a functional form whose local kinetic energy density is as close as possible to τ , it seems reasonable to follow the ansatz of Deb and Ghosh, cf. Eq. (4), and search for a density-based function $f(\mathbf{r})$, which sufficiently well reproduces the ELF kernel. Defining shell boundaries by maximal values of the ELF kernel yields a proper atomic shell structure for the whole Periodic Table [20]; therefore, the aim is to find such an indicator which follows this assumption, also revealing shell boundaries by maximal values. As will be shown below, one of those indicators is the charge-restricted dim-q, measuring the density inhomogeneity in so-called microcells controlled by fixed charge condition derived within the concept of ω -restricted space partitioning ω -RSP [52–54].

ELF was first defined for separate spin channels [32]. Later, several choices on how to construct an ELF formula for combined spin channels were proposed [20]. In the following, dim-q will be derived for separate spin channels as

well, so that f^α and f^β of Eq. (4) are allowed to differ from each other for spin-polarized systems.

For the model of a piecewise exponential electron density [55, 56] for given spin channel σ , whereby the electron density ρ^σ of each shell is given by a single exponential function, the shell boundaries will be revealed by a discontinuity in the electron density gradient, changing from one exponential behavior to the next one. Of course, the behavior of the real atomic density is smooth, but still relatively abrupt changes of the density occur at the shell boundaries. Thus, the shell boundaries can be detected by measuring how much the electron density changes in a given interval. Moreover, a relative measure should be used, comparing all results with respect to a fixed condition, since the decay of the electron density is of course highest at the nucleus and decreases monotonically. A relative measure comparing the electron density changes with respect to the electronic charge in this region reveals the desired shell boundaries [23, 57, 58].

According to the concept of ω -RSP the space is divided into compact, mutually exclusive space-filling regions, called microcells. In sufficiently small microcells μ_i , the σ -spin charge is directly proportional to the microcell volume V_i and the σ -spin electron density at the microcell center \mathbf{a}_i :

$$q_i^\sigma = \int_{\mu_i} \rho^\sigma(\mathbf{r}) dV \approx \rho^\sigma(\mathbf{a}_i) V_i. \quad (17)$$

A σ -spin charge-restricted ω -RSP is such a space partitioning that all microcells contain the same fixed amount of σ -spin charge ω_q^σ , the so-called control property, whereby the microcell volume is given by:

$$V_i \approx \frac{\omega_q^\sigma}{\rho^\sigma(\mathbf{a}_i)}. \quad (18)$$

The inhomogeneity $I_p^\sigma(i)$ [23, 57, 58] of the σ -spin electron density within such microcell is defined for any positive measure p as the distance between the σ -spin electron density and its averaged (homogeneous) value $\bar{\rho}_i^\sigma$ within this microcell:

$$I_p^\sigma(i) = \sqrt[p]{\int_{\mu_i} |\rho^\sigma(\mathbf{r}) - \bar{\rho}_i^\sigma|^p d\mathbf{r}}. \quad (19)$$

In sufficiently small microcells, the inhomogeneity is proportional to the electron density gradient and a power of the microcell volume, whereby the exponent depends on the chosen distance measure p [23, 57, 58]:

$$I_p^\sigma(i) \approx \frac{1}{2(p+1)^{1/p}} |\nabla \rho^\sigma(\mathbf{a}_i)| V_i^{(p+3)/3p}. \quad (20)$$

Now, if those volumes are chosen to be the volumes of the σ -spin charge-restricted space partitioning, cf. Eq. (17),

then the electron density inhomogeneity of given σ -spin channel in regions each containing the same amount of σ -spin charge is given by:

$$I_p^\sigma(i) \approx \frac{1}{2(p+1)^{1/p}} |\nabla \rho^\sigma(\mathbf{a}_i)| \left[\frac{\omega_q^\sigma}{\rho^\sigma(\mathbf{a}_i)} \right]^{(p+3)/3p}. \quad (21)$$

The value of the electron density inhomogeneity of course depends on the chosen restriction value ω_q^σ . In order to obtain an information independent of the chosen restriction value, the electron density inhomogeneity is rescaled by the proper power of the restriction value. The σ -spin charge-restricted density-inhomogeneity measure of ω -RSP microcells (dim-q) is defined as:

$$\iota_p^\sigma(\mathbf{a}_i) = \frac{I_p^\sigma(i)}{\left[\omega_q^\sigma \right]^{(p+3)/3p}}. \quad (22)$$

The limit after rescaling for $\omega_q^\sigma \rightarrow 0$ is a continuous function [54]:

$$\iota_p^\sigma(\mathbf{r}) = \frac{1}{2(p+1)^{1/p}} \frac{|\nabla \rho(\mathbf{r})|}{[\rho^\sigma(\mathbf{r})]^{(p+3)/3p}}. \quad (23)$$

Bear in mind that $\iota_p^\sigma(\mathbf{r})$ is in general not a dimensionless quantity, since the dimension of the electron density inhomogeneity $[I_p^\sigma(i)] = \text{length}^{(-3p+3)/p}$ depends on the distance measure p , cf. Eq. (19). The function $\iota_1^\sigma(\mathbf{r})$ as well as $I_1^\sigma(i)$ is dimensionless only for $p = 1$.

Notice that

$$\iota_1^\sigma(\mathbf{r}) = \frac{1}{4} \frac{|\nabla \rho(\mathbf{r})|}{[\rho^\sigma(\mathbf{r})]^{4/3}} \quad (24)$$

is proportional to the reduced density gradient, measuring variation of the density on the scale of the local Fermi wavelength [59]. However, the inhomogeneity concept of ι_p^σ is much broader, since it allows taking different measures p . Functions of the type ι_p^σ exhibit proper real space shell structure description for the whole Periodic Table over a large range of p values [57]. The optimal description with respect to the electronic population in the atomic shells is reached for p values between 0.6 and 1.14 yielding an average population deviation [21] of 0.4 electrons when compared to the ideal shell populations [19], see hashed area in Fig. 4.

Since for certain p values the shell boundaries of ι_p^σ are in close vicinity to the ideal shell boundaries, a suitable ansatz for representing the modifying function, cf. Eq. (4), in terms of ι_p^σ is:

$$f(\mathbf{r}) = \left(\iota_p^\sigma(\mathbf{r}) \right)^m, \quad (25)$$

with $(\iota_p^\sigma(\mathbf{r}))^m$ exhibiting the same shell structure as the indicator $\iota_p^\sigma(\mathbf{r})$.

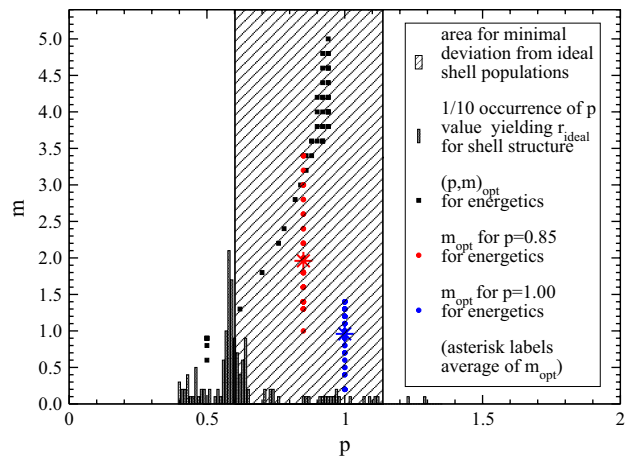


Fig. 4 Performance of SSB functionals using functions of type $t_{\text{test}} = t_W + (\iota_p^\sigma)^m t_{\text{TF}}$ with respect to the atomic shell structure and energetic aspects for different values of the parameter set (p, m)

The energetic performance of SSB functionals using functions of type $t_{\text{test}} = t_W + (\iota_p^\sigma)^m t_{\text{TF}}$ was examined for the atoms Li to Xe, whereby the optimal parameter values (p, m) were determined by least-square fit to the positive kinetic energy density τ . The data are shown by black squares in Fig. 4. Nearly all optimal data points lie within the p range leading to the optimal shell structure description, represented by the hashed area. Within this area, the averaged population deviation is 0.4 electrons, when a given p is chosen for the function ι_p^σ —in that case the p value is fixed for all shell boundaries.

The occurrences of ideal p values yielding shell separators exactly at the ideal positions are given by the gray bars at the bottom part of the figure (the data are divided by factor 10 for better visibility)—in that case p can differ for different shell boundaries of an atom, which of course cannot be represented by the ansatz of Eq. (25). However, the spread of the three different datasets is quite small, revealing that a proper atomic shell description also provides the best energetic description for the chosen ansatz. The blue- and red-colored points in Fig. 4 display the optimal m value for the atoms Li to Xe yielding the lowest quadratic deviation of the test function to τ for $p = 0.85$ and $p = 1$, respectively. The average of those optimal m values is indicated by an asterisk. For $p = 1$ the average of optimal m values is 0.96. However, $t_{\text{test}} = t_W + (\iota_p^\sigma)^m t_{\text{TF}}$ with $(p = 0.85, m = 1.96)$ provides a much better energetic description, as shown in Figs. 5, 6 and 7.

Figure 5 comprises the ELF kernel elf_τ (evaluated from HF orbitals) as well as four $(\iota_p^\sigma)^m$ -based approximative ELF kernels, cf. Eq. (25), with $(p = 1, m = 1)$, $(p = 1, m = 0.96)$, $(p = 0.85, m = 1)$ and $(p = 0.85, m = 1.96)$, respectively. All approximative ELF kernels display the proper number of shell boundaries

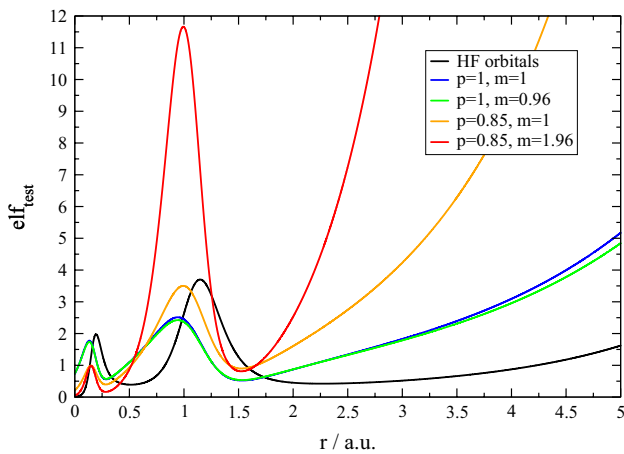


Fig. 5 Approximative ELF kernels for the Si atom obtained from the kinetic energy densities of SSB functionals using $t_{\text{test}} = t_W + (t_p^\sigma)^m t_{\text{TF}}$ for different values of (p, m)

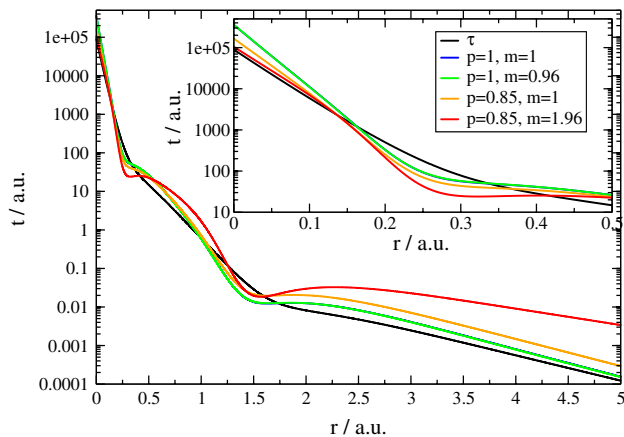


Fig. 6 Kinetic energy densities for the Si atom from the SSB functionals using $t_{\text{test}} = t_W + (t_p^\sigma)^m t_{\text{TF}}$ for different values of (p, m)

(given by the maxima of the functions) in close vicinity to the corresponding elf_τ shell boundaries. All functions $(t_p^\sigma)^m$ have a good overall correspondence with the ELF kernel elf_τ , whereby the two functions $(t_1^\sigma)^m$ are more suitable to mimic the long range behavior of elf_τ compared with their counterparts with $p = 0.85$. However, the energetic performance of $t_{\text{test}} = t_W + (t_p^\sigma)^m t_{\text{TF}}$ is mostly determined by the regions close to the nucleus, where $(t_1^\sigma)^m$ has much too high values compared with elf_τ . As a consequence of this, the corresponding kinetic energy densities, cf. Fig. 6, are too high in the vicinity of the nucleus, leading to much too high total kinetic energies and large oscillations in $\Delta T(r)$; see Fig. 7.

Despite their inadequate long range behavior, the functions $(t_{0.85}^\sigma)^m$ perform better close to the nucleus and

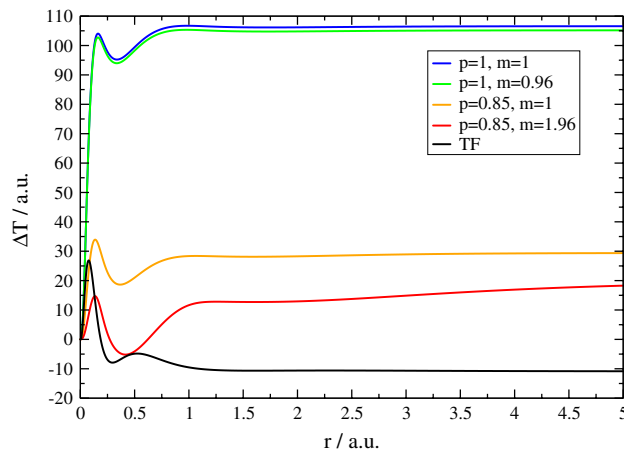


Fig. 7 Local contributions to the difference between the kinetic energy evaluated from orbitals and the approximative kinetic energy ($\Delta T(r) = \int_0^r 4\pi r^2 [t_{\text{test}}(r) - \tau(r)] dr$) for the Si atom from the SSB functionals using $t_{\text{test}} = t_W + (t_p^\sigma)^m t_{\text{TF}}$ for different values of (p, m)

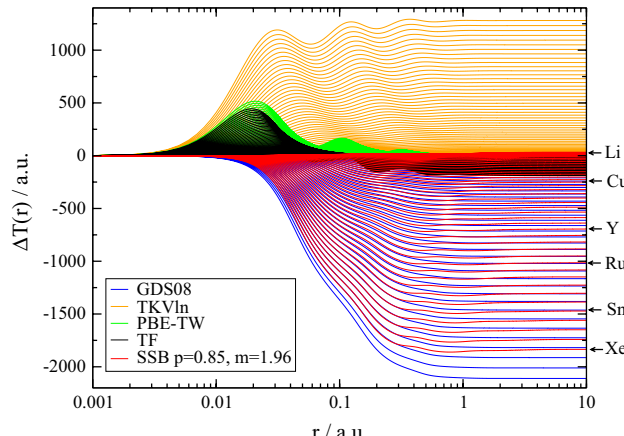


Fig. 8 Local contributions to the difference between the kinetic energy evaluated from orbitals and the approximative kinetic energy ($\Delta T(r) = \int_0^r 4\pi r^2 [t_{\text{test}}(r) - \tau(r)] dr$) for the atoms Li to Xe atom using various functionals

consequently, the corresponding kinetic energy densities are closer to τ as shown in Fig. 6. The overestimation of the total kinetic energy is significantly reduced up to 20 and 14 % for $(p = 0.85, m = 1)$ and $(p = 0.85, m = 1.96)$, respectively. Out of the tested functions, $(t_{0.85}^\sigma)^{1.96}$ displays the smallest oscillations in $\Delta T(r)$, and therefore, this function is a suitable approximation for τ when piecewise corrections are needed.

This trend is observed for all atoms from Li to Xe; see the red-colored solid lines in Fig. 8, with $\Delta T(r)$ evaluated for $t_{\text{test}} = t_W + (t_{0.85}^\sigma)^{1.96} t_{\text{TF}}$. For all atoms, the $\Delta T(r)$ curve for the $(t_{0.85}^\sigma)^{1.96}$ -based SSB functional exhibits the

Table 1 Kinetic energy of majority component for atoms from Li to Xe using various functionals

Atom	<i>T</i>	<i>T_W</i>	<i>T_{TF}</i>	<i>T_{PW91}</i>	<i>T_{DPK}</i>	<i>T_{Thakkar}</i>	<i>T_{TPBE-TW}</i>	<i>T_{GDS08}</i>	<i>T_{GHDS10}</i>	<i>T_{GHDS10-repar}</i>	<i>T_{TKVln}</i>	<i>T_{SSB-1}</i>	<i>T_{SSB-2}</i>
Li	3.8	3.6	3.4	3.8	3.8	3.8	3.8	3.9	8.0	7.1	7.1	8.5	17.4
Be	7.3	6.8	6.6	7.3	7.2	7.3	7.3	7.5	14.7	13.5	13.5	16.1	25.6
B	12.6	10.9	11.3	12.5	12.4	12.5	12.5	12.1	24.3	22.3	22.3	26.4	35.0
C	20.1	15.8	18.1	19.9	19.8	19.9	19.9	18.0	37.0	34.1	34.0	39.7	45.7
N	30.0	21.7	27.5	30.0	30.0	30.1	30.1	25.0	53.6	49.5	49.4	56.4	57.8
O	39.9	28.6	36.6	40.0	39.9	40.0	40.0	32.4	69.9	65.5	65.4	74.6	69.7
F	51.4	36.5	47.1	51.4	51.2	51.4	51.4	40.7	88.6	83.8	83.8	95.5	82.5
Ne	64.3	45.3	58.9	64.3	64.1	64.2	64.3	49.9	109.5	104.5	104.4	118.9	96.4
Na	81.1	55.2	74.5	81.2	81.0	81.1	81.1	59.9	135.5	130.1	130.0	146.9	111.1
Mg	99.8	66.3	92.0	100.0	99.8	99.9	100.0	71.6	164.5	158.7	158.6	178.0	127.9
Al	121.2	78.3	111.9	121.5	121.2	121.3	121.4	84.1	197.2	190.7	190.6	212.5	145.7
Si	145.4	91.4	134.5	145.7	145.4	145.4	145.6	97.9	233.8	226.4	226.3	250.5	165.1
P	172.4	105.5	159.9	172.9	172.6	172.5	172.8	113.1	274.5	266.0	265.9	292.2	185.8
S	200.6	120.7	186.2	201.1	200.8	200.6	201.0	128.9	316.4	307.5	307.4	336.3	206.6
Cl	230.8	136.9	214.5	231.4	231.1	230.8	231.3	145.6	361.3	351.9	351.8	383.5	228.4
Ar	263.4	154.2	245.0	264.1	263.8	263.3	263.9	163.5	409.5	399.8	399.7	434.2	251.5
K	299.7	172.6	278.9	300.5	300.0	299.4	300.2	181.9	462.2	452.1	452.0	488.8	274.4
Ca	338.4	192.0	315.0	339.1	338.6	337.9	338.7	202.1	518.3	507.7	507.6	546.9	299.9
Sc	381.4	212.1	355.0	381.7	381.2	380.2	381.3	223.3	579.6	567.9	567.7	608.5	325.6
Ti	428.1	233.2	398.6	428.0	427.4	426.2	427.5	245.5	645.5	632.5	632.4	673.8	352.4
V	478.6	255.2	445.9	478.2	477.6	476.1	477.7	269.0	716.2	702.0	701.8	742.9	380.5
Cr	534.3	277.9	499.1	534.4	533.7	531.9	533.8	293.6	794.3	778.0	777.8	816.4	409.1
Mn	591.1	302.2	553.0	591.5	590.6	588.6	590.8	319.0	873.3	856.2	856.0	893.2	439.9
Fe	645.8	327.5	604.3	646.1	645.1	642.9	645.3	344.8	950.3	932.9	932.7	971.1	470.9
Co	705.6	354.2	660.7	706.0	704.9	702.4	705.1	371.9	1033.7	1015.9	1015.7	1054.2	503.4
Ni	762.6	381.3	714.1	762.9	761.6	758.9	761.9	399.6	1114.6	1096.5	1096.3	1136.7	535.9
Cu	819.8	409.7	767.4	819.9	818.5	815.6	818.8	428.0	1196.3	1178.1	1178.0	1222.0	569.2
Zn	888.9	439.2	832.9	889.2	887.7	884.5	888.0	458.3	1291.9	1273.2	1273.0	1315.3	605.1
Ga	962.0	469.7	902.2	962.6	960.9	957.3	961.3	489.4	1392.6	1373.0	1372.9	1412.7	641.3
Ge	1038.9	501.2	975.2	1039.8	1037.9	1033.9	1038.3	521.9	1498.2	1477.6	1477.5	1514.1	679.2
As	1119.6	533.8	1052.0	1121.0	1118.8	1114.4	1119.3	555.7	1608.9	1587.1	1586.9	1619.6	718.3
Se	1202.0	567.5	1130.3	1203.6	1201.2	1196.5	1201.8	590.1	1721.3	1699.1	1698.9	1728.0	758.2
Br	1287.5	602.4	1211.5	1289.5	1286.8	1281.7	1287.5	625.7	1838.0	1815.2	1815.0	1840.1	799.2
Kr	1376.0	638.4	1295.6	1378.3	1375.4	1369.8	1376.2	662.3	1958.5	1935.3	1935.1	1955.8	841.4
Rb	1469.3	675.2	1384.2	1471.9	1468.7	1462.6	1469.6	699.4	2084.5	2060.8	2060.6	2076.0	882.9
Sr	1565.7	713.4	1476.0	1568.7	1565.2	1558.7	1566.2	738.3	2215.0	2190.8	2190.5	2200.0	927.4
Y	1666.9	752.3	1571.9	1669.9	1666.1	1659.0	1667.2	778.2	2351.0	2325.7	2325.5	2328.0	972.1
Zr	1773.7	792.2	1673.5	1776.8	1772.7	1765.0	1773.9	819.6	2494.3	2467.3	2467.0	2460.5	1018.3
Nb	1883.7	833.3	1778.3	1887.1	1882.7	1874.4	1884.0	862.1	2641.7	2613.3	2613.0	2596.9	1066.1
Mo	1998.2	875.4	1887.6	2002.0	1997.2	1988.3	1998.7	905.7	2794.5	2764.7	2764.5	2737.4	1114.9
Tc	2115.4	918.8	1999.4	2119.6	2114.4	2104.8	2116.0	950.1	2950.4	2920.0	2919.7	2881.7	1165.0
Ru	2229.3	963.2	2107.6	2233.7	2228.2	2218.1	2230.0	994.9	3103.3	3072.6	3072.4	3026.8	1215.0
Rh	2349.5	1008.6	2222.0	2354.2	2348.2	2337.5	2350.2	1040.9	3263.6	3232.4	3232.2	3176.8	1266.7
Pd	2468.9	1055.2	2335.3	2473.7	2467.4	2456.0	2469.5	1088.0	3423.4	3392.3	3392.0	3328.6	1320.5
Ag	2599.2	1102.7	2459.7	2604.3	2597.6	2585.6	2599.9	1136.1	3596.1	3564.2	3563.9	3487.7	1373.0
Cd	2732.0	1151.4	2586.1	2737.3	2730.2	2717.4	2732.6	1185.7	3771.9	3739.3	3739.1	3650.3	1428.2
In	2870.5	1201.1	2718.2	2876.1	2868.5	2854.9	2871.1	1236.1	3954.6	3921.2	3921.0	3817.4	1484.0
Sn	3012.7	1251.9	2853.9	3018.6	3010.6	2996.2	3013.4	1287.8	4142.2	4107.8	4107.6	3988.7	1541.2

Table 1 continued

Atom	T	T_W	T_{TF}	T_{PW91}	T_{DPK}	$T_{Thakkar}$	T_{PBE-TW}	T_{GDS08}	T_{GHDS10}	$T_{GHDS10\text{-repar}}$	T_{TKVln}	T_{SSB-1}	T_{SSB-2}
Sb	3159.2	1303.7	2993.6	3165.3	3156.8	3141.5	3159.8	1340.7	4334.9	4299.4	4299.1	4164.0	1599.5
Te	3307.9	1356.7	3135.3	3314.1	3305.1	3289.0	3308.3	1394.5	4530.2	4494.1	4493.8	4342.7	1658.8
I	3460.2	1410.8	3280.4	3466.5	3457.0	3440.0	3460.4	1449.4	4730.0	4693.4	4693.1	4525.2	1719.3
Xe	3616.0	1466.0	3428.9	3622.4	3612.3	3594.4	3615.9	1505.3	4934.1	4897.0	4896.7	4711.5	1780.9
$\bar{\Delta}_{\text{abs}}$		634.7	64.8	1.9	0.9	5.7	0.4	616.0	616.0	449.3	449.2	442.8	487.3
$\bar{\Delta}_{\text{rel}}$		0.5	0.1	0.002	0.002	0.004	0.001	0.4	0.4	0.5	0.5	0.6	0.5

The kinetic energies using the SSB functionals T_{SSB-1} and T_{SSB-2} are evaluated with the parameter set ($p = 1.00, m = 0.96$) ($p = 0.85, m = 1.96$), respectively. $\bar{\Delta}_{\text{abs}}$ and $\bar{\Delta}_{\text{rel}}$ are the mean absolute error and the mean relative error, respectively

fewest oscillations close to the nucleus, meaning that, out of the examined functional set, for this functional the kinetic energy density is locally closest to τ . However, the integrated values may differ largely for heavier atoms, comparing also data in Table 1, since a SSB functional incorporates the influence of the Pauli exclusion principle and the errors due to the chosen approximation accumulate for each shell. Starting from second-row elements, the underestimation of T_P is found to be systematic, so that the $\Delta T(r)$ curves for the SSB functional (red solid lines) are ordered with respect to the atomic number, with Xe showing the largest difference to T ; see Fig. 8. By the way, this observation holds for all tested functionals, except the chosen GGA functional (T_{PBE-TW}). For the atoms Li to Cu, the energetic performance of $t_{\text{test}} = t_W + (\iota_{0.85}^{\sigma})^{1.96} t_{TF}$ is comparable to that of t_{TF} . Beginning with Cu, the kinetic energy is significantly underestimated by the proposed SSB functional, but the performance is still better than the one of T_{GDS08} ; see the blue-colored solid lines in Fig. 8. In contrast, the functional T_{TKVln} largely overestimates the influence of the Pauli repulsion, as can be seen from the orange-colored solid lines. The typical GGA-like behavior of $\Delta T(r)$ is exemplarily demonstrated by the dataset (shown in green) of T_{PBE-TW} . The errors for the total energy are small for all atoms, but the local correspondence between the kinetic energy densities and τ is even worse than that between t_{TF} and τ (data shown in black).

As a solid-state example, $t_{\text{test}} = t_W + (\iota_{0.85}^{\sigma})^{1.96} t_{TF}$ was calculated for Si in the diamond structure. Figure 9 displays the kinetic energy densities for τ , t_{test} and t_{TF} as well as the ELF kernel elf_{τ} calculated from KS orbitals together with the approximative ELF kernel arising from t_{test} along the diagonal of the unit cell, so that the bond critical point (bcp) of the shortest Si–Si distance is located at the right part of the figure. As can be seen, the function $(\iota_{0.85}^{\sigma})^{1.96}$ mimics the shell structure as given by ELF kernel elf_{τ} . Differences arise at the critical points of the electron density (ring critical point at $r = 0$ bohr, cage critical point at $r = 2.2$ bohr, bcp at $r = 8.8$ bohr), where t_{test} is zero irrespective of the chosen (p, m) parameter values. However, in those regions the positive kinetic energy density is usually

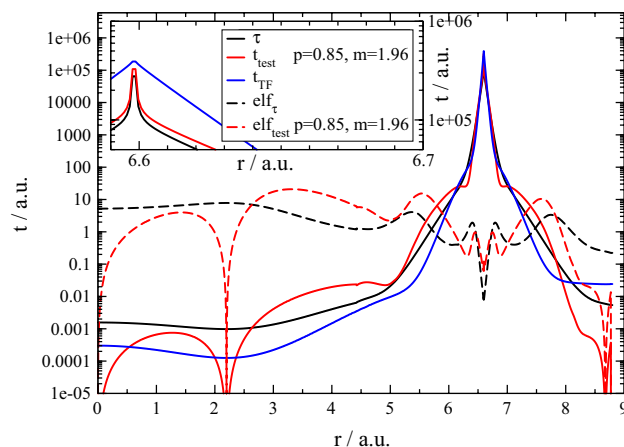


Fig. 9 Comparison of kinetic energy densities for Si in the diamond structure along the diagonal of the unit cell. The bond midpoint for the shortest Si–Si distance is located at the right part of the figure

very small. The integration of $t_{\text{test}} = t_W + (\iota_{0.85}^{\sigma})^{1.96} t_{TF}$ over the unit cell yields for one spin component the approximative kinetic energy $T_t = 319$ a.u. overestimating by 10 % only the kinetic energy $T = 290$ a.u. (for comparison $T_{TF} = 268$ a.u., $T_W = 183$ a.u.). Notice the remarkable local correspondence between $t_{\text{test}} = t_W + (\iota_{0.85}^{\sigma})^{1.96} t_{TF}$ and τ for the solid-state calculation. Even the relativistic effects nearby the Si nucleus are captured by the proposed SSB functional; see inset of Fig. 9.

5 Conclusions

This study provides a new systematic route for the design of kinetic energy density functionals. It utilizes the direct connection between the Pauli enhancement factor and the electron localization function (ELF), which is known to be a prominent quantitative atomic shell descriptor. Purely density-based shell descriptors, which sufficiently well mimic ELF, give rise to new kinetic energy functionals termed shell-structure-based functionals (SSB).

Based on the idea of an ideal piecewise exponential decaying density, a purely density-based shell indicator was derived, which measures the electron density inhomogeneity in regions of fixed electronic charge. The inhomogeneity was defined as the distance between the electron density and its averaged (homogeneous) value in so-called microcells. Since the distance between two functions can be determined using various measures, the resulting inhomogeneity concept bears a measure parameter p . Suggesting a simple m -power form, the proposed approximative ELF kernel is $(t_p^\sigma)^m$ with the corresponding kinetic energy density expressed as $t_{\text{test}} = t_W + (t_p^\sigma)^m t_{\text{TF}}$ including two parameters (p, m). It was shown that parameter values leading to a proper description of the atomic shell structure give rise to reasonable kinetic energy functionals. The optimal parameters ($p = 0.85, m = 1.96$) were determined by least-square fit of t_{test} to τ for the atoms Li to Xe. The resulting kinetic energy functional was applied to a self-consistent KS electron density for Si in diamond structure. For this solid-state example, the proposed SSB functional overestimates the kinetic energy by 10 % only. Local changes in τ due to relativistic effects were also captured by the proposed SSB functional.

Acknowledgments My grateful thanks to Miroslav Kohout for personal encouragement, fruitful discussions and carefully reading the manuscript. The Alexander von Humboldt foundation is greatly acknowledged for funding this work.

References

- Karasiev V, Jones RS, Trickey SB, Harris FE (2009) Recent advances in developing orbital-free kinetic energy functionals. In: Paz EJ, Hernandez AJ (eds) New developments in quantum chemistry. Transworld Research Network, Trivandrum
- Karasiev VV, Trickey SB (2012) Comput Phys Commun 183:2519–2527
- Karasiev V, Chakraborty D, Trickey SB (2013) Progress on new approaches to old ideas: orbital-free density functionals. In: Delle Site L, Bach V (eds) Many-electron approaches in physics, chemistry and mathematics: a multidisciplinary view. Springer, Berlin
- Shin I, Carter EA (2014) J Chem Phys 140:18A531
- Xia J, Carter EA (2015) Phys Rev B 91:045124
- Thomas LH (1927) Proc Cambridge Philos Soc 23:542–548
- Fermi E (1928) Z Phys 48:73–79
- von Weizsäcker CF (1935) Z Phys 96:431–458
- Kirzhnits DA (1957) Sov Phys JETP 5:64–71
- Hodges CH (1973) Can J Phys 51:1428–1437
- Tran F, Wesolowski TA (2002) Int J Quantum Chem 89:441–446
- Ghiringhelli LM, Delle Site L (2008) Phys Rev B 77:073104
- Ghiringhelli LM, Hamilton IP, Delle Site L (2010) J Chem Phys 132:014106
- Trickey S, Karasiev VV, Vela A (2011) Phys Rev B 84:075146
- Wang YA, Carter EA (2000) Orbital-free kinetic-energy density functional theory. In: Schwarz SD (ed) Theoretical methods in condensed phase chemistry. Kluwer, NY, pp 117–184
- Bartell LS, Brockway LO (1953) Phys Rev 90:833–838
- Waber JT, Cromer DT (1965) J Chem Phys 42:4116–4123
- Boyd RJ (1976) J Phys B 9:69–72
- Schmid H, Sagar R, Smith VH Jr (1992) Can J Chem 70:506–512
- Kohout M, Savin A (1996) Int J Quantum Chem 60:875–882
- Finzel K, Kohout M (2013) Theor Chem Acc 132:1392
- Finzel K (2014) Int J Quantum Chem 114:1546–1558
- Finzel K, Grin Y, Kohout M (2012) Theor Chem Acc 131:1106
- Deb BM, Ghosh SK (1983) Int J Quantum Chem 23:1–26
- Hohenberg P, Kohn W (1964) Phys Rev B 136:864–871
- Yonei K, Tomishima Y (1965) J Phys Soc Jpn 20:1051–1057
- Alonso JA, Girifalco LA (1978) Chem Phys Lett 53:190–191
- Tal Y, Bader RFW (1978) Int J Quantum Chem S12:153–168
- Yang W (1986) Phys Rev A 34:4575–4585
- Yang W, Parr RG, Lee C (1986) Phys Rev A 34:4586–4590
- Savin A, Jepsen O, Flad J, Anderson OK, Preuss H, von Schnering HG (1992) Angew Chem Int Ed 31:187–188
- Becke AD, Edgecombe KE (1990) J Chem Phys 92:5397–5403
- Tsirelson VG, Stash AI (2002a) Acta Crystallogr B Struct Sci 58:780–785
- Tsirelson VG, Stash AI (2002b) Chem Phys Lett 351:142–148
- Tsirelson VG, Stash AI (2002c) Acta Crystallogr B Struct Sci 58:632–639
- Stash AI, Tsirelson VG (2005) Crystallogr Rep 50:177–184
- Ayers PW (2005) J Chem Sci 117:441–454
- Parr GR, Yang W (1989) Density-functional theory of atoms and molecules. Oxford University Press, Oxford
- Zhao Q, Parr RG (1992) Phys Rev A 46:2337–2343
- Szabo A, Ostlund NS (1996) Modern quantum chemistry—introduction to advanced electronic structure theory. Dover Publications Inc., Mineola
- Grling A, Ernzerhof M (1995) Phys Rev A 51:4501–4513
- Kohout M, Savin A (1997) J Comput Chem 18:1431–1439
- Kohout M (2010) DGrid, version 4.6. Radebeul
- Clementi E, Roetti C (1974) At Data Nucl Data Tables 14:177–478
- Elk (2009) <http://elk.sourceforge.net/>
- Lacks DJ, Gordon RG (1994) J Chem Phys 100:4446–4452
- DePristo AE, Kress JD (1987) Phys Rev A 35:438–441
- Thakkar AJ (1992) Phys Rev A 46:6920–6924
- Cohen L (1984) J Chem Phys 80:427–4279
- Ayers PW, Parr RG, Nagy A (2002) Int J Quantum Chem 90:309–326
- Anderson JSM, Ayers P, Hernandez JIR (2010) J Phys Chem A 114:8884–8895
- Kohout M (2004) Int J Quantum Chem 97:651–658
- Kohout M (2007) Faraday Discuss 135:43–54
- Martín Pendás A, Kohout M, Blanco MA, Francisco E (2012) Beyond standard charge density topological analyses. In: Gatti C, Macchi P (eds) Modern charge density analyses. Springer, London
- Weinstein H, Politzer P, Srebrenik S (1975) Theor Chim Acta 38:159–163
- Wang WP, Parr RG (1977) Phys Rev A 16:891–901
- Finzel K (2011) Über die Entwicklung der Realraumindikatoren c_p . Ph.D. thesis, Technische Universität Dresden
- Wagner K, Kohout M (2011) Theor Chem Acc 128:39–46
- Perdew JP, Ernzerhof M, Zupan A, Burke K (1998) J Chem Phys 108:1522–1531